JOURNAL OF AIRCRAFT
Vol. 37, No. 3, May–June 2000

Simulation of Store Separation for the F/A-18C Using Cobalt$_{60}$

Robert F. Tomaro,* Frank C. Witzeman,* and William Z. Strang*
Air Force Research Laboratory, Wright–Patterson Air Force Base, Ohio 45433

A demonstration is presented of the ability of computational fluid dynamics (CFD) methods to predict store carriage loads and support store trajectory generation. A complete, complex aircraft, the F/A-18C, was modeled with actual stores in their carriage positions. Cobalt$_{60}$, a parallel, implicit unstructured flow solver, was used to calculate the flowfield and resultant aerodynamic loads on grids composed of tetrahedral cells. Three grids were used to simulate three different flowfield approximations. Because of lateral symmetry, only the right half was modeled. The first grid was a purely inviscid grid containing 3.15 million cells. The second grid was made up of 3.96 million cells clustered to capture viscous effects on only the store components. The third grid was a full viscous grid containing 6.62 million cells. Store carriage loads for two flight conditions were calculated and compared with wind-tunnel measurements and flight-test data for each of the preceding grids. The resulting carriage loads were used in a separate six-degree-of-freedom rigid-body motion code to generate store trajectories. All CFD solutions were second-order accurate and run to steady state with Courant–Friedrichs–Lewy numbers of one million. Turnaround times ranged from 6 to 21 h, depending on the number of processors used.

Nomenclature

C_A = axial force coefficient, positive aft
C_l = rolling moment coefficient, positive clockwise when looking upstream
C_m = pitching moment coefficient, positive nose up
C_N = normal force coefficient, positive up
C_n = yawing moment coefficient, positive nose inboard
C_Y = side force coefficient, positive right (inboard)
p = roll rate, deg/s
q = pitch rate, deg/s
r = yaw rate, deg/s
x_{cg} = JDAM c.g. location, x axis, in.
y_{cg} = JDAM c.g. location, y axis, in.
z_{cg} = JDAM c.g. location, z axis, in.
θ = body-axis pitch angle, deg
ϕ = body-axis roll angle, deg
ψ = body-axis yaw angle, deg

Introduction

THE incorporation of computational fluid dynamics (CFD) tools into the store certification process is limited at the present. Accurate, reliable answers must be provided quickly and economically. First, the entire solution process must be accomplished in a matter of days. With the maturing of the unstructured grid-generation process, full viscous grids can be generated in under a week's time on very complex configurations. Using massively parallel supercomputers and convergence acceleration techniques, turbulent solution CPU times on unstructured grids have been reduced to a number of hours. Unstructured grids also have the inherent ability to be decomposed into equal or nearly equal subsections. This quality translates into perfect or near perfect load balance allowing the efficient use of massively parallel supercomputers.

The U.S. Air Force SEEK EAGLE ACFD (Applied Computational Fluid Dynamics) project wants to provide the store separation engineer with accurate, reliable, and efficient CFD tools. From a CFD developer's point of view, capturing the fluid physics and resulting aerodynamics accurately with quick turnaround time is the goal. For store integration and certification obtaining accurate carriage loads in a timely manner is very important. If this is accomplished, then CFD has demonstrated one of its relative contributions. Trajectory generation/analysis, ejector modeling, etc. are separate technology areas that are best addressed by store certification experts.

Past demonstrative efforts have used several combinations of grid and flow solver techniques. Accurate predictions of store carriage loads on a generic wing/pylon/finned-store configuration[1–5] were presented in 1992. These results were mostly Euler calculations on a simple geometry. In 1996 a more complex aircraft/store configuration was studied, the F-16/generic finned-store.[6–8] However, questions about the accuracy of the wind-tunnel measurements were raised in that study. In addition, incorporating CFD tools into the certification process has been slowed by a lack of validations and demonstrations on real configurations.

The F/A-18C Joint Direct Attack Munition (JDAM) MK-84 configuration was chosen for this study because both wind-tunnel measurements and flight-test data exist. For the flight test both photogrametrics and telemetry were used to track the flight path of the released JDAM. The wind-tunnel test used a 6% scale F/A-18C model. Both a captive trajectory system (CTS) and a fixed pylon-mounted JDAM approach were used in the wind tunnel. During the CTS experiment, the JDAM was supported by a six-degree-of-freedom mechanism that enabled motion independent of the aircraft. The CTS-based and fixed-carriage wind-tunnel measurements correlated well with each other at only a few select conditions.[9] JDAM trajectories generated from these data were compared with flight-test values, and an inverse approach was used to determine the actual carriage loads that matched flight-test trajectories.[9]

This paper describes the JDAM aerodynamic loads and trajectory results obtained using the U.S. Air Force Research Laboratory (AFRL) Cobalt$_{60}$ flow solver and the Naval Air Warfare Center (NAWC) NAVSEP trajectory generator. Overviews of each method are provided in the following sections, and flowfield and trajectory results at two Mach numbers are given in the final sections.

Overview of Cobalt$_{60}$

Cobalt$_{60}$ is a parallel, implicit unstructured flow solver developed by the Computational Sciences Branch of AFRL.[10] Godunov's first-order accurate, exact Riemann method[11] is the foundation of Cobalt$_{60}$. Second-order spatial accuracy, second-order-accurate implicit time stepping, viscous terms, and turbulence models have been added to this procedure. Cobalt$_{60}$ uses a finite volume, cell-centered approach. Arbitrary cell types in two or three dimensions may be used, and a single grid may be composed of a variety of cell types. For three-dimensional flows cell types include, but are not limited to, tetrahedrons, prisms, pyramids, and hexahedrons. Typical cell types

Received 22 May 1999; revision received 9 September 1999; accepted for publication 13 September 1999.

*Aerospace Engineer, Computational Sciences Branch, Air Vehicles Directorate.

for two dimensions are triangles and quadrilaterals. Information on the calculation of inviscid and viscous fluxes and the dissipation in Cobalt$_{60}$ is reported in Strang et al.[10] Two one-equation turbulence models have been implemented in Cobalt$_{60}$, the Spalart–Allmaras[12] model and the Baldwin–Barth model.[13]

The implicit algorithm in Cobalt$_{60}$ was implemented and demonstrated by Tomaro et al.[14] The implicit algorithm resulted in a 5–10 times speed up over the original explicit algorithm with only a 10% increase in memory. Inviscid flows were routinely obtained with CFL numbers of one million; however, turbulent flows severely limited the CFL number. A further modification to the original implicit algorithm, reported by Strang,[10] removed the limitation for viscous flows, allowing CFL numbers of one million for most problems. This modified implicit algorithm resulted in a 7–10 times speed up in convergence over the original explicit code for viscous flows.

The development of the parallel version of Cobalt$_{60}$ was reported by Grismer et al.[15] Domain decomposition is the basis for the parallel code. Each processor operates on a subsection (zone) of the original grid. Information is passed between processors using the Message Passing Interface (MPI) library routines. Cobalt$_{60}$ has been implemented and tested on IBM SP2s, Cray T3Es, and SGI Origin 2000s. The resulting speed up of Cobalt$_{60}$ demonstrated superscalability on large cache-based systems, i.e., the speed-up factor was greater than the number of processors used.

Cobalt$_{60}$ allows a variety of boundary conditions.[16] For these F/A-18C simulations the far field was imposed using a modified Riemann invariant method. The surfaces of the body were slip walls for an inviscid surface or adiabatic no-slip walls for a viscous surface. To account for flow through the engine, a source/sink pair was used. The engine face used a corrected mass flow sink boundary condition to enforce the mass flowing out of the grid at this boundary surface. The engine exhaust was modeled with a source boundary condition to allow flow into the domain from this boundary surface.

Grid Resolution/Physics Study

Three separate grids were constructed to simulate the flowfield around the F/A-18C with stores. Lateral symmetry enabled modeling of only the right portion of the configuration. These three grids were used for a resolution study as well as a level of physics study. The equation set used in the simulation impacts the solution time as well as the aerodynamics. Therefore, it is important to know which level of physics is required for an engineering analysis. To that end, an inviscid solution, a stores-only viscous solution, and a full viscous solution were calculated and compared. All three grids modeled the complete F/A-18C including the inlet duct to the engine face, the boundary-layer diverter with flow through to the upper surface of the wing, the stair-stepped pylons, and the strakes on the JDAM including the notches.

The fully inviscid grid contained 3.15 million tetrahedral cells. Cobalt$_{60}$ required approximately 2.4 Gb of memory for this case. The grid was generated using Gridtool and VGRIDns[17]; both programs have been developed by NASA Langley Research Center. The F/A-18C was essentially the first grid attempted with VGRIDns by the first author. The first step is to construct patches over the original PLOT3D surfaces. The same surface patching was used as a basis for all three grids. The second step is to place sources to control grid spacing and clustering. This is an iterative step until the desired spacing is achieved. The third step is to triangulate the surface patches and project them onto the original PLOT3D surfaces. The final step is to generate the volume mesh; this step required approximately 1 h on an SGI Octane workstation.

The second grid treated the surfaces of the JDAM and fuel tank as viscous surfaces. The rest of the aircraft was simulated with slip walls. This grid was generated using the inviscid surface patching but setting the boundary condition of the JDAM and fuel tank surfaces to be viscous. VGRIDns will then generate viscous layers off these surfaces. The second grid contained 3.96 million tetrahedral cells with approximately 850,000 cells in the boundary layer requiring approximately 6.0 Gb of memory for this case. The generation of the volume grid again required 1 h of CPU time. Essentially, the same grid clustering was used as that for the fully inviscid case.

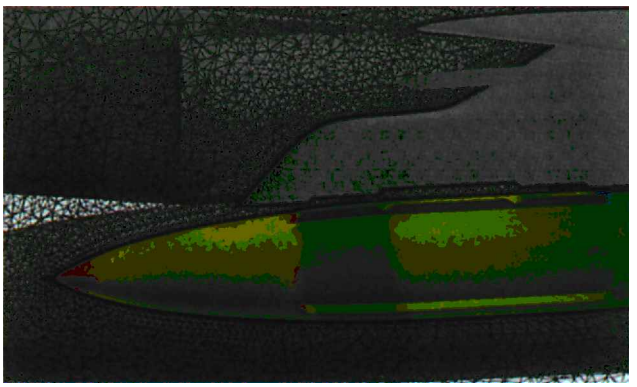

Fig. 1 Viscous grid near the JDAM and the outboard pylon.

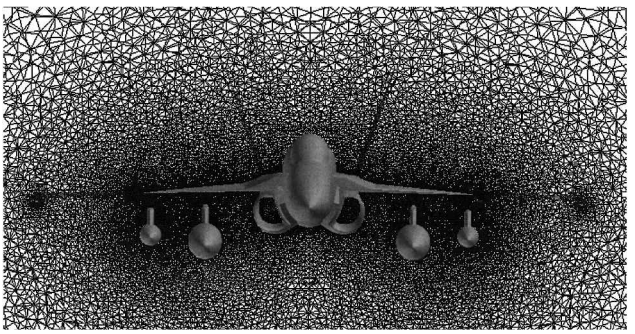

Fig. 2 Viscous grid clustering at a fuselage station through the JDAM.

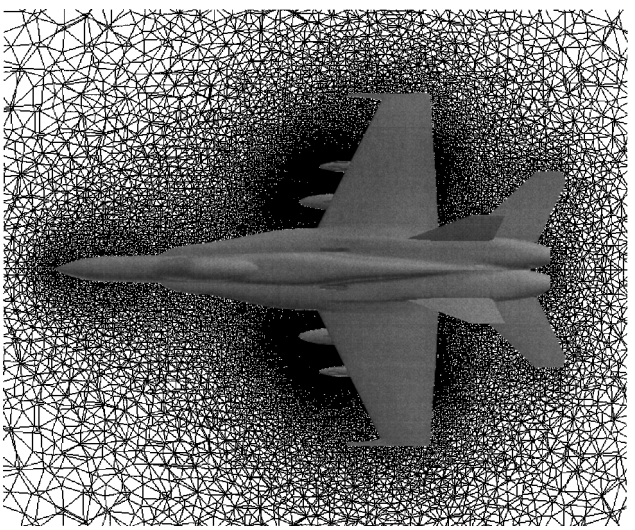

Fig. 3 Viscous grid clustering at a water line through the JDAM.

The full viscous grid contained 6.62 million tetrahedral cells including approximately 4 million cells in the boundary layer. This grid was constructed by specifying all surface patches of the inviscid grid as now being viscous. For the full viscous case Cobalt$_{60}$ required approximately 10.1 Gb of memory. The full viscous grid spacing around the JDAM and outboard pylon is shown in Fig. 1. Figures 2 and 3 show the viscous grid clustering at a fuselage station and a water line of the aircraft, respectively. Note that the grid has been reflected about the symmetry plane to illustrate the full configuration. The JDAM is the outboard store, and the fuel tank is the inboard store.

Overview of NAVSEP

Store trajectories may be obtained when carriage loads and isolated store aerodynamics are provided to an independent six-degree-of-freedom, rigid-body motion solver. For this F/A-18C JDAM

Table 1 JDAM properties input to NAVSEP

Property	Value
Weight	2059.44 lb (934.14 kg)
Length	152.4 in. (3.87 m)
c.g. location (x, y, z)	453.084, 134.28, 69.795 in. (11.51, 3.41, 1.773 m)
Forward ejector location	442.974 in. (11.251 m)
Forward ejector force	4680 lb (20,818 N)
Aft ejector location	462.974 in. (11.760 m)
Aft ejector force (peak)	4680 lb (20,818 N)
Ejector stroke lengths (2 Stages)	0.524, 6.015 in. (0.013, 0.153 m)
Roll moment of inertia, Ixx	20.02 slug-ft^2 (27.39 kg-m^2)
Pitch moment of inertia, Iyy	406.56 slug-ft^2 (551.21 kg-m^2)
Yaw moment of inertia, Izz	406.59 slug-ft^2 (551.25 kg-m^2)
Product of inertia, Ixz (= Izx)	−0.68 slug-ft^2 (−0.92 kg-m^2)
Product of inertia, Ixy (= Iyx)	0.86 slug-ft^2 (1.17 kg-m^2)
Product of inertia, Iyz (= Izy)	0 slug-ft^2 (0 kg-m^2)
Roll damping coefficient	−3/rad
Pitch damping coefficient	−141/rad
Yaw damping coefficient	−126/rad

effort AFRL obtained and used the NAWC NAVSEP trajectory generation program (private communication by A. Cenko, January 1998). This code is used routinely by the U.S. Navy, and it requires minimal computer resources and user intervention requirements. NAVSEP is based on the Arnold Engineering Development Center (AEDC) trajectory generation system[18] embedded in its captive trajectory testing setup. The program integrates the standard conservation of linear and angular momentum equations for a rigid body experiencing aerodynamic and other body forces and moments (see Ref. 18 for a description of the equations).

The use of NAVSEP in this study was limited to JDAM trajectory generations based on Cobalt$_{60}$-derived aerodynamics (carriage and freestream), Navy-supplied ejector modeling, and JDAM inertial properties. Table 1 summarizes the store property inputs required.

In addition to the JDAM aerodynamics and preceding properties, information related to a decay function must be supplied to NAVSEP. This function varies with lateral and vertical distance of a store with respect to the carriage position such that the carriage loads dominate the effective aerodynamic forces and moments at and near the initial release point. Later, the loads decay to the freestream, isolated store aerodynamics. Typically the vertical separation distance is much larger than the lateral displacement, and when a store falls anywhere from 7 to 10 body diameters away, it is considered to be outside the carriage influence region.

Results

Two flight conditions were simulated on the three grids. The first test case was at Mach number $M_\infty = 0.962$ with $\alpha = 0.46$ deg at an altitude of 6332 ft. The second flight condition was an altitude of 10,832 ft with a Mach number $M_\infty = 1.055$ and $\alpha = -0.65$ deg. The Spalart–Allmaras turbulence model was used in the viscous cases. For these simulations the right side of the aircraft was modeled. The x axis runs aft from the nose to the tail; the y axis is positive out the right wing; and the z axis is positive upward. Because the flight test tracked the JDAM on the left wing, there will be some sign changes required to match the CFD results, the wind-tunnel measurements, and the flight-test data. The geometric reference quantities used to obtain the aerodynamic coefficients are presented in Table 2.

Flowfield: $M_\infty = 0.962$

All three grids were used in the transonic simulations. An example of typical convergence history is shown in Fig. 4. Each simulation was run 2000 iterations, but the solutions are converged by 800 iterations. These forces are reported in the body-axis system of the entire aircraft.

In addition to grid clustering, Fig. 1 shows pressure contours on the JDAM. A high-pressure region exists at the nose because of the stagnation point. There is another high-pressure region at the beginning of the JDAM module; this JDAM module appears to have a sheet metal base that is attached only to the store itself. The JDAM module also includes the strakes. The high-pressure region is caused by the thickness of this sheet medal plate acting as a forward facing ramp, which was obviously modeled in the grids. The flow then expands as this ramp becomes parallel with the store surface again causing a lower-pressure region. A shock aft of this position causes another pressure rise.

Table 2 Geometric reference quantities for JDAM aerodynamic forces and moments, aircraft reference axes

Property	Value
Reference area	254.45 in^2. (0.164 m^2)
Moment reference length	
(x axis)	18.0 in. (0.457 m^2)
(y axis)	18.0 in. (0.457 m^2)
(z axis)	18.0 in. (0.457 m^2)
Moment reference center (at JDAM c.g.)	453.084, 134.28, 69.795 in. (11.51, 3.41, 1.773 m)

Table 3 JDAM right-wing carriage loads for $M_\infty = 0.962$, Cobalt$_{60}$ aircraft axis system

Coefficient	Inviscid	Viscous stores	Viscous
C_N	0.1408	0.1280	0.1122
C_A	0.6467	0.6921	0.7014
C_Y	−0.2992	−0.3136	−0.2843
C_m	−1.9807[a]	−2.1668[a]	−2.1697[a]
C_n	−2.2706[a]	−2.4630[a]	−2.4515[a]
C_l	0.1695[a]	0.1826[a]	0.1796[a]

[a]Incorrect reference location: $x_{cg} = 453.08$ in. (11.51 m), $y_{cg} = 134.28$ in. (3.41 m), $z_{cg} = 66.51$ in. (1.69 m).

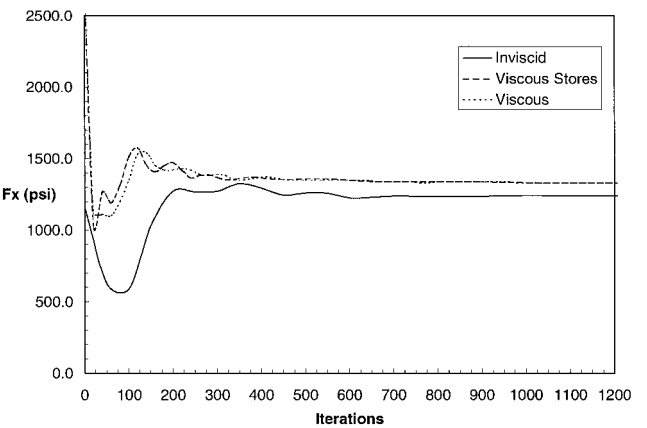

Fig. 4 Convergence history of axial force on the JDAM, $M_\infty = 0.962$.

Table 3 compares the JDAM force and moment coefficients for this flight condition. The moments were taken about an incorrect reference center location with respect to the z axis, which was corrected prior to the trajectory simulations. The coefficients are further referenced to the aircraft axis system already discussed and are not consistent with the JDAM body-axis definitions used for the wind-tunnel or flight-test data. The normal force has decreased with the addition of viscous forces. Axial force has been increased in the viscous simulations as expected. Side force varied slightly in the three different simulations. There are significant changes in the forces and moments between the inviscid simulation and the viscous simulations. However, the forces and moments vary slightly between the viscous stores simulation and the full viscous simulation. Therefore, to predict accurately the carriage loads for an engineering analysis, treating only the stores as viscous seems sufficient.

The inviscid case was simulated on 32 processors of an IBM SP2. The wall clock time was 4.90 h, the solution time per CPU was 4.87 h, and the total CPU time was 155.84 h. The viscous stores grid was run on 36 processors of an IBM SP2. This solution required a

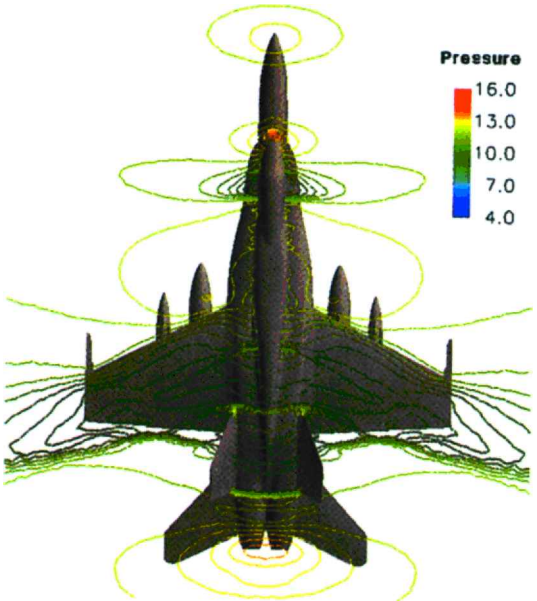

Fig. 5 Pressure contours at water line = 135 in. (3.43 m), $M_\infty = 0.962$.

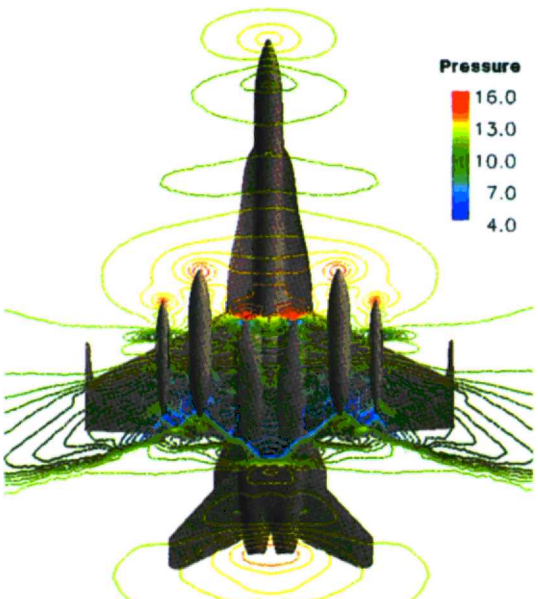

Fig. 6 Pressure contours at water line = 72 in. (1.83 m), $M_\infty = 0.962$.

wall clock time of 4.85 h, 4.72 h for each CPU and a total CPU time of 169.78 h. The viscous stores simulation had an average y^+ of 4.38. The full viscous case used 50 IBM SP2 processors. This simulation had an average y^+ of 3.65. The wall clock time required was 17.69 h. The total CPU time was 861.0 h with each CPU requiring 17.22 h. The preceding times are for converged solutions at 800 iterations.

Figure 5 shows pressure contours at a water line of 135 in. (3.43 m), a position above the F/A-18C wing. Notable flow features include the expansion around the front half of the canopy, a shock wave near the middle of the canopy, and shock waves aft of the boundary-layer diverter. Because the flow has accelerated to supersonic speeds over the upper fuselage, a shock wave exists in front of the vertical tails caused by their presence. The interesting shock is the normal shock between the trailing edges of the vertical tails. Figure 6 shows the complex flowfield interactions below the wing at a water-line station of 72 in. (1.83 m), which intersects the JDAM and fuel tank. The expansions caused by the JDAM module and the shock wave on the module can clearly be seen. A low-pressure region between the aft ends of the fuel tank and the JDAM gives rise to the inboard pointing side force. Aft of the two stores there are a series of intersecting oblique shocks that the released JDAM must pass through.

Table 4 JDAM body-axis carriage loads for $M_\infty = 0.962$

Coefficient	Value
C_N	0.0753
C_A	0.7063
C_Y	0.2844
C_m	−2.2854
C_n	−2.4403
C_l	0.0177

Trajectory: $M_\infty = 0.962$

The JDAM carriage loads from the viscous Cobalt_{60} simulation (see Table 3) were transformed to the correct store body-axis reference system. This system is aligned with the JDAM body axis, which is pitched down 3 deg with respect to the aircraft axis and is centered at the JDAM c.g. location. A further simple transformation was required to determine forces and moments for the left-wing configuration. The final carriage results, listed in Table 4, are consistent with the flight-test configuration where the x axis points forward along the JDAM centerline, the y axis points inboard, and the z axis points downward. The normal force is positive in the negative z direction, and the axial force is positive in the negative x direction. The pitching moment coefficient from Cobalt_{60} of $C_m = -2.2854$ matches the carriage and CTS wind-tunnel measurements of $C_m = -2.3$, (see Cenko[9] for all flight-test data and wind-tunnel measurements). The Cobalt_{60} yawing moment coefficient result of $C_n = -2.4403$ falls in the range of the carriage $C_n = -2.80$ and CTS measurement of $C_n = -1.55$. Cobalt_{60} calculated a side force coefficient of $C_Y = 0.2844$, which slightly underpredicts the flight-test and wind-tunnel values of $C_Y = 0.31$. The normal force coefficients were measured as $C_N = 0.15$ for the flight test and $C_N = 0.105$ for the wind tunnel, which are slightly larger than the Cobalt_{60} value of $C_N = 0.0753$. Overall, the carriage loads from Cobalt_{60} matched very well with the flight-test and wind-tunnel data.

A series of 5-alpha and 5-beta sweeps for the isolated JDAM were also conducted with Cobalt_{60}, and the numerical results were placed in a data table for NAVSEP. All of the required JDAM properties from Table 1 and other input parameters such as altitude and Mach number were also supplied. Trajectory results using decay functions based on 7–10 diameters and time-step increments of 0.005 s exhibited large discrepancies when compared to the flight-test data. Time-step increments below the value used did not improve the results. Therefore, the decay function was selected to eliminate the carriage loads effects after the JDAM had fallen about 1–1.5 diameters away from the pylon. This modification suggests that the aerodynamic loads on the JDAM in the transition region between carriage and the freestream are changing rapidly as strong flow gradients exist in the early stages of release. A grid-based aerodynamic data matrix or a fully integrated, moving-mesh CFD capability may be required to obtain more accurate trajectories.

Predicted JDAM trajectory parameters are compared to the flight-test telemetry and photogrametric data in Figs. 7–9. The axial and vertical displacements are underpredicted, whereas the pitch and yaw angles are overpredicted. A roll reversal occurs during the ejection sequence in flight, as shown by the data in Fig. 9; therefore, the roll angle and roll rate are not well predicted by the simple ejector model used in NAVSEP.

The predicted pitch rate overshoots the maximum flight-test value at about 0.14 s (see Fig. 9) and then recovers by 0.25 s. The predicted yaw rate recovers more rapidly than the flight-test values, which indicate a nearly flat rate between 0.15–0.25 s.

Flowfield: $M_\infty = 1.055$

Simulations on the three grids were completed for the supersonic case. An example of typical convergence history is shown in Fig. 10. Each simulation was run 2000 iterations, but the solutions were

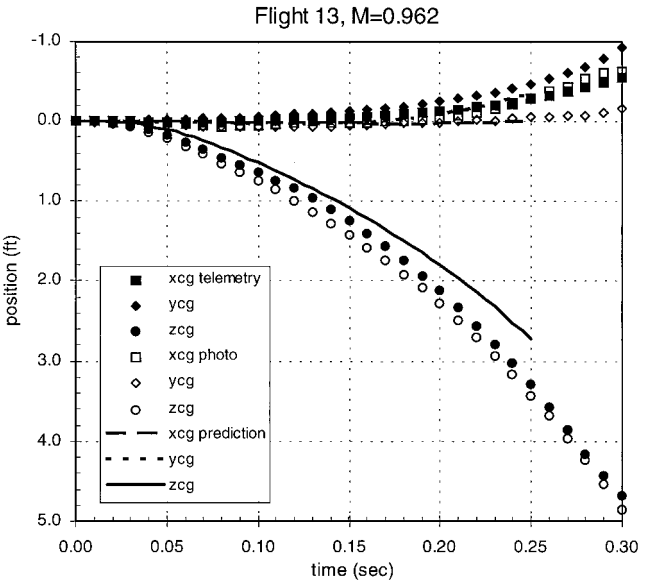

Fig. 7 JDAM c.g. locations, $M_\infty = 0.962$.

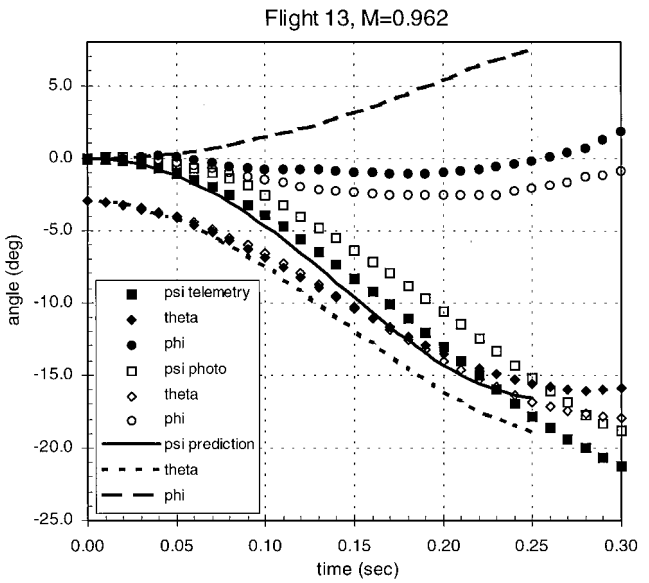

Fig. 8 JDAM attitudes, $M_\infty = 0.962$.

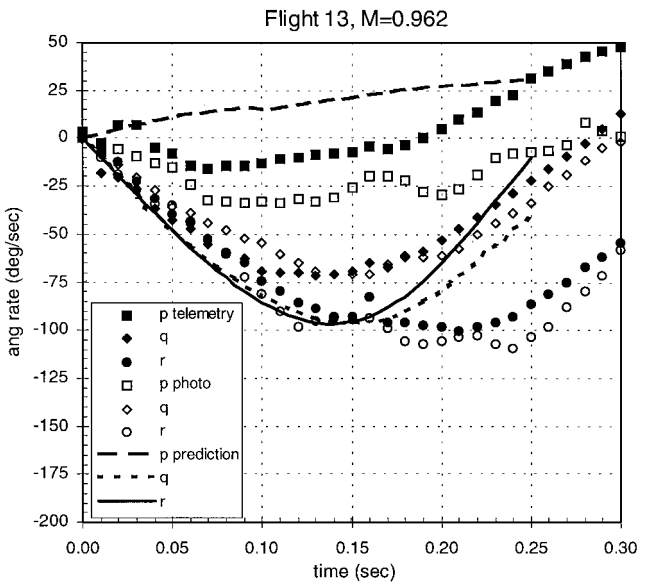

Fig. 9 JDAM angular rates, $M_\infty = 0.962$.

Table 5 JDAM right-wing carriage loads for $M_\infty = 1.055$, $Cobalt_{60}$ aircraft axis system

Coefficient	Inviscid	Viscous stores	Viscous
C_N	0.0840	0.0347	0.0224
C_A	0.6236	0.6826	0.6873
C_Y	−0.2728	−0.2825	−0.2572
C_m	−1.9362[a]	−2.0835[a]	−2.0651[a]
C_n	−2.0465[a]	−2.2403[a]	−2.1909[a]
C_l	0.1908[a]	0.4346[a]	0.2019[a]

[a]Incorrect reference location: $x_{cg} = 453.08$ in. (11.51 m), $y_{cg} = 134.28$ in. (3.41 m), $z_{cg} = 66.51$ in. (1.69 m).

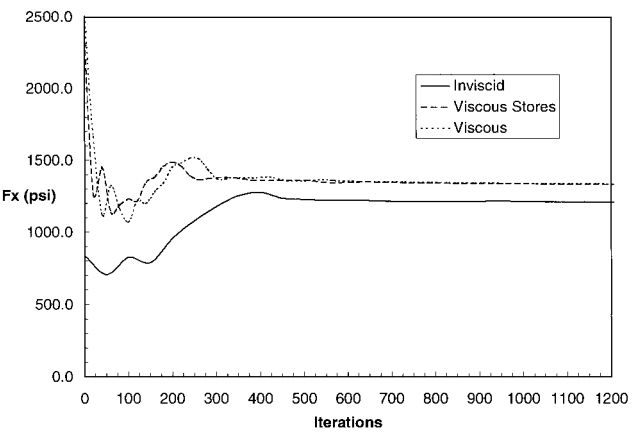

Fig. 10 Convergence history of axial force on the JDAM, $M_\infty = 1.055$.

again converged by 800 iterations. The axial force is reported in the body-axis system of the entire aircraft.

The JDAM carriage force and moment comparisons for the three grid systems are presented in Table 5. Note that the moments were again taken about an incorrect reference location (which was corrected prior to the trajectory simulations), and the reference axis was for the aircraft. The same changes in magnitudes of the forces were seen for this case as for the $M_\infty = 0.962$ flight condition. Again, there are significant changes in the forces and moments between the inviscid simulation and the viscous simulations but slight changes between the viscous stores simulation and the full viscous simulation. For an engineering analysis only the stores need to be treated as viscous surfaces.

The inviscid case was simulated on 32 processors of an IBM SP2. The wall clock time was 4.95 h, the solution time per CPU was 4.92 h, and the total CPU time was 157.57 h. The viscous stores grid required 4.84 h of wall clock time, 4.70 h on each CPU, and 169.34 h of total CPU time. The solution was run on 36 processors of an IBM SP2. The viscous stores simulation had an average y^+ of 4.12. The full viscous case used 32 IBM SP2 processors. This simulation had an average y^+ of 3.46. The wall clock required time was 26.87 h. The total CPU time was 840.0 h with each CPU requiring 26.27 h. The preceding times are for converged solutions at 800 iterations.

Figure 11 shows pressure contours at a water line of 135 in. (3.43 m), a position above the F/A-18C wing. Shock waves exist in front of the nose and in front of the canopy, and a well-defined shock is positioned in front of the wing because of blockage effects. As in the $M_\infty = 0.962$ case, shocks sit after the boundary-layer diverter and before the vertical tails. A relatively strong shock sits at the aft end of the aircraft. Figure 12 shows the complex flowfield interactions below the wing at a water-line station of 72 in., (1.83 m) which intersects the JDAM and fuel tank. As in the $M_\infty = 0.962$ case, expansion and shock waves on the JDAM module can clearly be seen. A low-pressure region between the aft ends of the fuel tank and the JDAM causes the inboard-pointing side force. Aft of the two stores, there is another series of intersecting oblique shocks, which the released JDAM passes through. These oblique shocks are further aft than those of the $M_\infty = 0.962$ case.

Figure 13 shows the F-18C surface colored by pressure. The solution is for the full viscous simulation at $M_\infty = 1.055$. High pressure

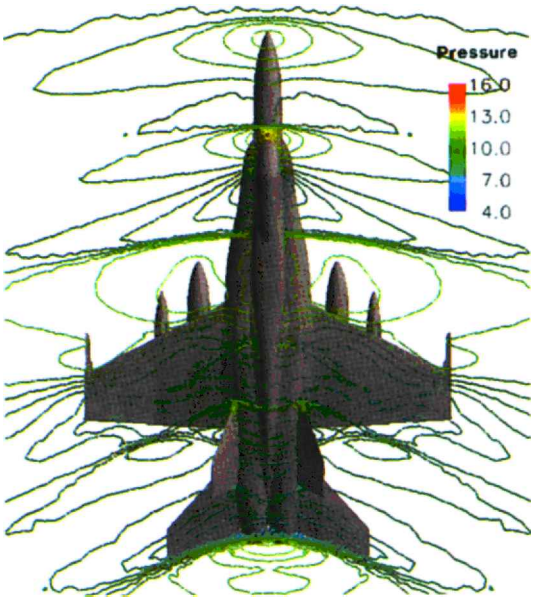

Fig. 11 Pressure contours at water line = 135 in. (3.43 m), $M_\infty = 1.055$.

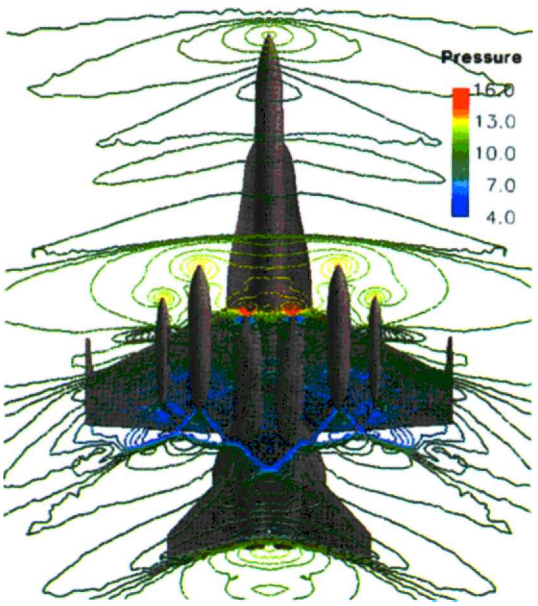

Fig. 12 Pressure contours at water line = 72 in. (1.83 m), $M_\infty = 1.055$.

is shown in red and low pressure in blue. The shock wave after the canopy as shown in Figs. 11 and 12 is clearly seen on the surface in Fig. 13. The effects of complex flow interactions between the wing, pylons, and stores can be seen by this surface-pressure distribution.

The JDAM carriage loads from the fully viscous case (see Table 5) were transformed to the JDAM body-axis system already described. Because the CFD simulation modeled the right side of the aircraft, it was necessary to change the sign of the side force coefficient to provide loads consistent with the flight-tested left-wing configuration. The final carriage results are listed in Table 6. The x axis points forward along the JDAM centerline, the y axis points inboard, and the z axis points downward. The pitching moment coefficient for the carriage and CTS wind-tunnel measurements of $C_m = -2.15$, (see Cenko[9] for all flight-test data and wind-tunnel measurements) was slightly overpredicted by the Cobalt$_{60}$ value of $C_m = -2.2335$. The Cobalt$_{60}$ yawing moment coefficient result of $C_n = -2.2111$ falls in the range of the carriage $C_n = -2.60$ and CTS measurement of $C_n = -2.15$. Cobalt$_{60}$ predicted a side force coefficient of $C_Y = 0.2572$, which closely approximated the flight-test

Table 6 JDAM body-axis carriage loads for $M_\infty = 1.055$

Coefficient	Value
C_N	−0.0136
C_A	0.6876
C_Y	0.2572
C_m	−2.2335
C_n	−2.2111
C_l	0.0129

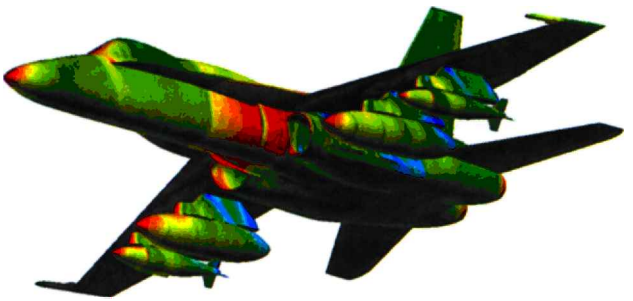

Fig. 13 Surface pressures on the F-18C at $M = 1.055$, viscous solution.

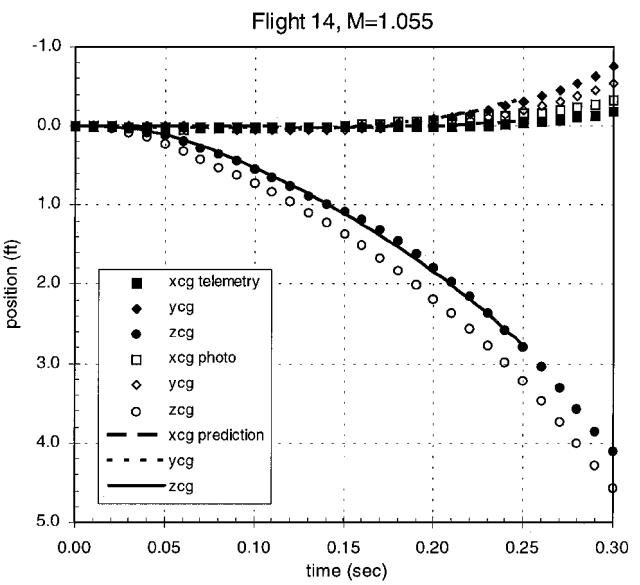

Fig. 14 JDAM c.g. locations, $M_\infty = 1.055$.

and wind-tunnel values of $C_Y = 0.25$. The normal force coefficients were measured as $C_N = 0.05$ for the flight test and $C_N = 0.03$ for the wind tunnel, which are slightly larger than the Cobalt$_{60}$ value of $C_N = -0.0136$. Overall, the carriage loads from Cobalt$_{60}$ matched very well with the flight- test and wind-tunnel data.

A series of 8-alpha and 5-beta sweeps for the isolated JDAM were also conducted with Cobalt$_{60}$, and the numerical results were placed in a data table for NAVSEP. Similar to the earlier Mach-number case, trajectory predictions using decay functions based on 7–10 diameters and time steps of 0.005 s exhibited large discrepancies when compared to the flight-test data. Again, the decay function was selected to eliminate the carriage loads effects after the JDAM had fallen about 1–1.5 diameters away from the pylon. Strong flow gradients exist in the early stages of release, and the transition region between carriage and freestream aerodynamics is difficult to predict. Grid-based studies, integrated moving-mesh CFD, or other influence-based means are required to obtain more accurate aerodynamics in the near-pylon region.

Resulting JDAM trajectory parameters are compared to the flight-test telemetry and photogrametric data in Figs. 14–16. Note that the c.g. displacements are well predicted, whereas the pitch and yaw

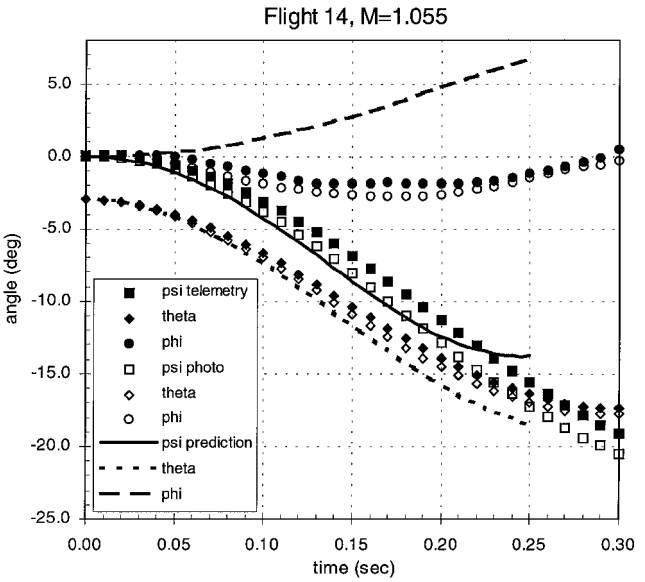

Fig. 15 JDAM attitudes, $M_\infty = 1.055$.

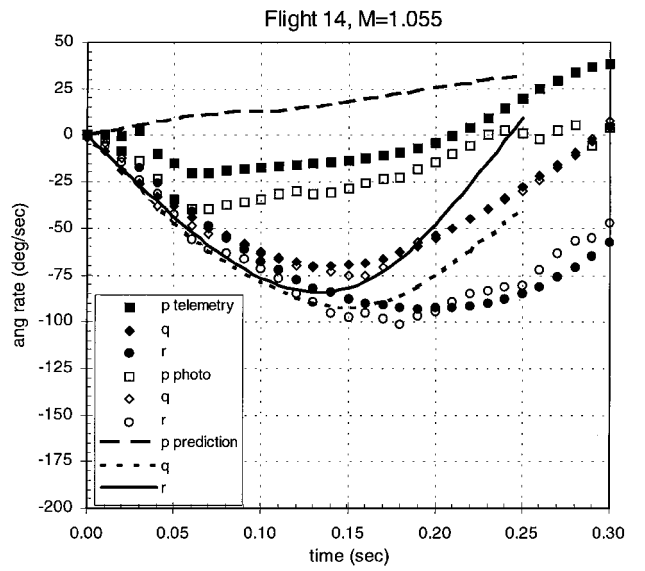

Fig. 16 JDAM angular rates, $M_\infty = 1.055$.

angles are overpredicted as in the preceding Mach number case. Again, a roll reversal occurs during the ejection sequence in flight (see Fig. 16); therefore, the roll angle and roll rate are not well predicted by the simple ejector model used in NAVSEP.

The predicted pitch rate overshoots the maximum flight-test value at about 0.15 s (see Fig. 16) and then recovers after 0.25 s. The predicted yaw rate recovers more rapidly than the flight-test values, and by 0.25 s this rate is increasing in the opposite direction. A sudden increase in predicted yaw angle, as shown in Fig. 15, results from the yaw rate reversal.

Conclusions

Store carriage loads for a complex air vehicle system were obtained accurately and rapidly using viscous unstructured-grid CFD methodology. The Cobalt$_{60}$ flow solver developed by the AFRL/Computational Sciences Branch was able to resolve relevant compressible, viscous flow features, which dictate the aerodynamic loading. The parallel processing feature in Cobalt$_{60}$ further enables rapid turnaround time for a single solution, such that in a week's time many carriage configurations may be simulated during a parametric investigation.

Store separation trajectories were generated with the NAWC's NAVSEP code, a separate rigid-body, six-degree-of-freedom motion solver. All CFD-based aerodynamics, as well as store inertial properties, were simply tabulated and input. The resulting trajectories correlated well with the flight-test data in the earliest stages of release, and then departed from the data when the carriage effects were considered to be diminished. Sources of such discrepancies were likely causesd by simple ejector modeling characteristics and general difficulties in determining suitable aerodynamics in regions of rapidly changing mutual interference between the store and parent vehicle.

Acknowledgments

The authors would like to thank J. Garriz and S. Pirzadeh for their help with VGRIDns. All of the simulations in this paper were run using the IBM SP2 located at the ASC/MSRC, Wright–Patterson Air Force Base, Ohio.

References

[1]Lijewski, L., and Suhs, N., "Chimera-Eagle Store Separation," AIAA Paper 92-4569, Aug. 1992.

[2]Meakin, R. L., "Computations of the Unsteady Flow About a Generic Wing/Pylon/Finned-Store Configuration," AIAA Paper 92-4568, Aug. 1992.

[3]Newman, J. C., and Baysal, O., "Transonic Solutions of a Wing/Pylon/Finned-Store Using Hybrid Domain Decomposition," AIAA Paper 92-4571, Aug. 1992.

[4]Parikh, P., Pirzadeh, S., and Frink, N. T., "Unstructured Grid Solutions to a Wing/Pylon/Store Configuration Using VGRID3D/USM3D," AIAA Paper 92-4572, Aug. 1992.

[5]Jordan, J. K., "Computational Investigation of Predicted Store Loads in Mutual Interference Flow Fields," AIAA Paper 92-4570, Aug. 1992.

[6]Madson, M., and Talbot, M., "F-16/Generic Carriage Load Predictions at Transonic Mach Numbers Using TRANAIR," AIAA Paper 96-2454, June 1996.

[7]Cline, D., Riner, W., Jolly, B., and Lawrence, W., "Calculation of Generic Store Separations from an F-16 Aircraft," AIAA Paper 96-2455, June 1996.

[8]Kern, S. B., and Bruner, C. W. S., "External Carriage Analysis of a Generic Finned-Store on the F-16 Using USM3D," AIAA Paper 96-2456, June 1996.

[9]Cenko, A., "F-18/JDAM CFD Challenge Wind Tunnel Flight Test Results," AIAA Paper 99-0120, Jan. 1999.

[10]Strang, W. Z., Tomaro, R. F., and Grismer, M. J., "The Defining Methods of Cobalt$_{60}$: A Parallel, Implicit, Unstructured Euler/Navier–Stokes Flow Solver," AIAA Paper 99-0786, Jan. 1999.

[11]Godunov, S. K., "A Difference Scheme for Numerical Computation of Discontinuous Solution of Hydrodynamic Equations," *Sbornik Mathematics*, Vol. 47, 1959, pp. 271–306.

[12]Spalart, P. R., and Allmaras, S. R., "A One-Equation Turbulence Model for Aerodynamic Flows," AIAA Paper 92-0439, Jan. 1992.

[13]Baldwin, B. S., and Barth, T. J., "A One-Equation Turbulence Transport Model for High Reynolds Number Wall-Bounded Flows," NASA TM 102847, Aug. 1990.

[14]Tomaro, R. F., Strang, W. Z., and Sankar, L. N., "An Implicit Algorithm for Solving Time Dependent Flows on Unstructured Grids," AIAA Paper 97-0333, Jan. 1997.

[15]Grismer, M. J., Strang, W. Z., Tomaro, R. F., and Witzeman, F. C., "Cobalt: A Parallel, Implicit, Unstructured Euler/Navier–Stokes Solver," *Advances in Engineering Software*, Vol. 29, No. 3–6, 1998, pp. 365–373.

[16]Strang, W. Z., "Parallel Cobalt$_{60}$ User's Manual," Air Force Research Lab./Computational Sciences Branch, Wright–Patterson AFB, OH, Aug. 1998.

[17]Pirzadeh, S., "Three-Dimensional Unstructured Viscous Grids by the Advancing-Layers Method," *AIAA Journal*, Vol. 34, No. 1, 1996, pp. 43–49.

[18]Carmen, J. B., Jr., Hill, D. W., Jr., and Christopher, J. P., "Store Separation Testing Techniques at the Arnold Engineering Development Center, Vol. 2, Description of Captive Trajectory Store Separation Testing in the Aerodynamic Wind-Tunnel (4T)," Arnold Engineering Development Center, AEDC-TR-79-1, June 1980.

Color reproductions courtesy of Computational Sciences Branch/AFRL.